Optimization of DRP schemes for non-constant-amplitude oscillations

Edward J. Brambley*
Mathematics Institute and WMG, University of Warwick, United Kingdom
Vilda K. Markevičiūtė†
Faculty of Mathematics, University of Cambridge, United Kingdom

It was recently observed that finite difference schemes optimized to perform well with few points per wavelength (commonly referred to as DRP schemes) currently perform poorly when applied to waves of non-constant amplitude. In this paper, attempts are described at optimizing explicit symmetric finite difference schemes to require relatively few points per wavelength for waves with a range of growth-rates and decay-rates. Several optimization criteria are proposed, and some advantage may be gained from using such optimized schemes if the growth- and decay-rates present are known a priori. In particular, for the test case considered here, the usual 7 point 4th order DRP schemes are found to be overly ambitious in their optimization, and better performing schemes are derived which require almost half the number of points per wavelength to achieve the same accuracy. Without a priori knowledge, however, the best choice of finite difference schemes for waves of varying amplitude remain the classical maximal order schemes.

I. Introduction

Due to the complex geometry and flow through and around an aircraft engine, Computational Aero-Acoustics (CAA) simulations place great demands on computational time and memory. A large range of CAA simulations are based on finite differences. For a 3D CAA simulation (at a fixed CFL number), moving from 5 to 6 points per wavelength would cause a 73% increase in memory usage and 107% increase in computational time. Consequently, significant research effort has been directed at finite difference derivatives that require the fewest points per wavelength to accurately resolve a wave[1–10].

We consider here explicit symmetric finite difference schemes on equally space grids $x_j = j\Delta x$. The theory below remains valid for implicit (i.e. compact) schemes, while a preliminary study for non-symmetric schemes is given in Ref. 11. Given a function $f(x)$ evaluated at discrete points $f_j = f(x_j)$, the derivative $f'(x_j)$ is approximated by a $2N+1$ point finite difference

$$f'_j = \frac{1}{\Delta x}\sum_{q=1}^{N} d_q(f_{j+q} - f_{j-q}). \tag{1}$$

It is hoped that f'_j is a close approximation of the actual derivative $f'(x_j)$ for sufficiently small Δx. If $f'_j = f'(x_j) + O\big(\Delta x^{2L}\big)$ as $\Delta x \to 0$, we say the derivate has $2L$th order accuracy. The coefficients d_q may be chosen uniquely to maximize the order of the derivative; such derivatives are referred to here as "maximal order" (MO), and give $L = N$. Substituting into (1) a wave with $f(x) = \mathrm{Re}\big(A\mathrm{e}^{\mathrm{i}\alpha x}\big)$ leads to the numerical prediction

$$f'_j = \mathrm{Re}(\mathrm{i}\bar{\alpha}A\mathrm{e}^{\mathrm{i}\alpha x_j}), \qquad \text{where} \qquad \bar{\alpha}\Delta x = 2\sum_{q=1}^{N} d_q \sin(q\alpha\Delta x). \tag{2}$$

*Associate Professor and Royal Society University Research Fellow, Mathematics Institute and WMG, University of Warwick, Coventry, CV4 7AL, United Kingdom. AIAA senior member.

†Undergraduate, Faculty of Mathematics, University of Cambridge, CMS, Wilberforce Road, Cambridge, CB3 0WA, United Kingdom. AIAA non-member.

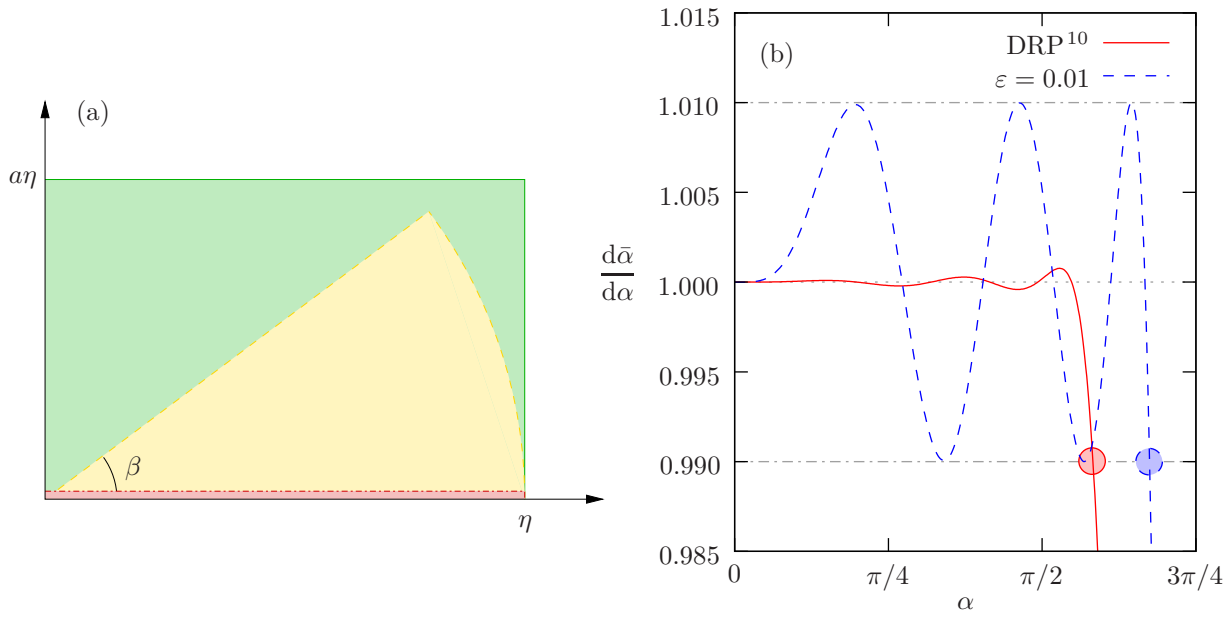

Figure 1: (a) Areas of the complex $\alpha\Delta x$ plane over which the numerical derivative will be optimized. The red area bounded by the dot-dash line shows the current DRP optimization only along the real α axis. The green area bounded by the solid line shows a rectangular optimization, while the yellow area bounded by the dashed line shows a sector of angle β, representing a maximum growth or decay per wavelength by a factor of $\exp\{2\pi\tan\beta\}$.
(b) Plots of $\mathrm{d}\bar{\alpha}/\mathrm{d}\alpha$ against α, both for $N = 7$ and $L = 2$. The DRP scheme is that of Tam [10], while the $\varepsilon = 0.01$ scheme is optimized for fewest points per wavelength for an error of $\varepsilon = 0.01$. Filled circles show the first position with a numerical group velocity error of over 0.01.

Clearly we would like $\bar{\alpha}$ to be as close to α as possible for wave problems. Tam & Webb [5] chose $N = 3$ but only required $L = 2$, giving a 7 point derivative of 4th order accuracy, and used the remaining degree of freedom to minimize

$$E = \int_0^\eta \left|\bar{\alpha}(\alpha)\Delta x - \alpha\Delta x\right|^2 \mathrm{d}(\alpha\Delta x) \tag{3}$$

with $\eta = \pi/2$. Subsequently, Tam & Shen [6] suggested $\eta = 1.1$ gives a more balanced scheme, and this scheme is widely used today. Such optimized schemes are commonly referred to as Dispersion Relation Preserving, or DRP, schemes.

The optimizations involved in generating DRP schemes to date assume that α is real, and hence that the oscillations are of constant amplitude. Recently, Brambley [12,13] considered non-constant-amplitude oscillations by allowing α to be complex, and showed that existing DRP schemes performed worse than maximal order schemes in such cases. This is not surprising, since schemes optimized to perform well for real α have no reason to perform well for non-real α. Unfortunately, non-constant-amplitude waves are rather common in aeroacoustics, especially when considering the performance of acoustic linings, where waves can decay by a factor of 25 or more over one wavelength [14]. The purpose of this paper is to consider re-optimizing DRP schemes with the aim of improving their ability to handle oscillations of non-constant-amplitude.

II. DRP optimization for non-constant-amplitude oscillations

A. Optimization over a range of complex α

One possibility to cover non-constant-amplitude oscillations is to generalize the error measure (3) to a region of complex α. Two shapes are considered here, as shown in figure 1(a). For a rectangular region of α, writing $\alpha\Delta x = p + \mathrm{i}q$ allows (3) to be generalized to

$$E = \frac{1}{a\eta}\int_0^{a\eta}\int_0^{\eta} \left|\bar{\alpha}((p+\mathrm{i}q)/\Delta x)\Delta x - (p+\mathrm{i}q)\right|^2 \mathrm{d}p\mathrm{d}q. \tag{4}$$

The parameter a here controls the range of numerical decay-rates or growth-rates of interest. As $a \to 0$ the constant-amplitude DRP schemes are recovered, while for $a \gg \eta$ schemes are optimized for pure exponential growth or decay without oscillation. Another possibility is to optimize over a disk centred on $\alpha = 0$, or indeed a sector of a disk. Writing $\alpha\Delta x = r\mathrm{e}^{\mathrm{i}\theta}$ gives such a generalization of (3) as

$$E = \frac{1}{\beta}\int_0^\beta \int_0^\eta \left|\bar{\alpha}(r\mathrm{e}^{\mathrm{i}\theta}/\Delta x)\Delta x - r\mathrm{e}^{\mathrm{i}\theta}\right|^2 r\mathrm{d}r\mathrm{d}\theta. \tag{5}$$

Here β controls the range of growth-rates or decay-rates of the underlying continuous system of interest, since changing Δx by coarsening or refining the numerical grid changes $|\alpha\Delta x|$ but leaves $\arg(\alpha\Delta x)$ unchanged; in other words, this optimizes over growth and decay rates per wavelength from $\exp\{-2\pi\tan\beta\}$ to $\exp\{2\pi\tan\beta\}$. As $\beta \to 0$ a differently-weighted version of the constant-amplitude DRP optimization (3) is recovered.

B. Optimization of group velocity and higher derivatives

The numerical group velocity error is defined[3,15] as

$$\varepsilon_g = \left|\frac{\mathrm{d}\bar{\alpha}}{\mathrm{d}\alpha} - 1\right|. \tag{6}$$

The group velocity error is an important quantification of the accuracy of numerical schemes in its own right, with Trefethen[15] saying that the group velocity error gives "a quantitative understanding of differencing errors in wave propagation problems, of the appearance of parasitic waves, ..., and of instability in initial boundary value problem". More relevant to the current discussion is that $\bar{\alpha}\Delta x$ is seen from (2) to be an analytic (complex differentiable) function of $\alpha\Delta x$. Hence, for real α_0,

$$\bar{\alpha}(\alpha_0 + \mathrm{i}\delta) = \bar{\alpha}(\alpha_0) + \mathrm{i}\delta\mathrm{d}\bar{\alpha}/\mathrm{d}\alpha + \cdots, \tag{7}$$

which will be close to $\alpha_0 + \mathrm{i}\delta$ provided both (a) $\bar{\alpha}$ is a good approximation of α for real α, and (b) $\mathrm{d}\bar{\alpha}/\mathrm{d}\alpha \approx 1$. Since phase velocity errors $|\frac{\bar{\alpha}}{\alpha} - 1|$ are commonly smaller than group velocity errors ε_g (see Ref. 3), (a) is commonly satisfied provided $\mathrm{d}\bar{\alpha}/\mathrm{d}\alpha \approx 1$, and so (b) is the limiting requirement. In other words, if the numerical group velocity is accurate along the real axis (equivalent to ε_g being small for real α), then the numerical wavenumber $\bar{\alpha}$ is close to α not only along the real axis but also in a neighbourhood of the real axis. Thus, an optimization minimizing ε_g (6) in some way for constant-amplitude oscillations, which is useful in its own right, could also be expected to give better results for non-constant-amplitude oscillations.

One option considered here is to minimize

$$E = \int_0^\eta \left|\frac{\mathrm{d}\bar{\alpha}}{\mathrm{d}\alpha} - 1\right|^2 \mathrm{d}(\alpha\Delta x), \tag{8}$$

which is the group velocity equivalent of the usual DRP phase velocity minimization (3). As an alternative, we also consider maximizing η such that ε_g is smaller than some given threshold ε for real $\alpha\Delta x < \eta$, as shown in figure 1(b); this alternative corresponds to minimizing the number of points-per-wavelength needed for a group velocity accuracy ε. This latter optimization results in a closed form expression for 7-point 4th order schemes ($N = 3$, $L = 2$), given in appendix A.1. In the limit $\varepsilon \to 0$ this appears to tend to the maximal order scheme.

Higher order derivatives of $\bar{\alpha}$ may also be considered by taking more terms of the Taylor series expansion (7). Below, results are presented for optimizations involving $\mathrm{d}^2\bar{\alpha}/\mathrm{d}\alpha^2$, with the equivalent of (8) then being

$$E = \int_0^\eta \left|\frac{\mathrm{d}^2\bar{\alpha}}{\mathrm{d}\alpha^2}\right|^2 \mathrm{d}(\alpha\Delta x). \tag{9}$$

Similarly, maximizing η such that $|\mathrm{d}^2\bar{\alpha}/\mathrm{d}\alpha^2| < \varepsilon$ for real $\alpha\Delta x < \eta$ is also attempted.

One might also consider combining the two approaches above by optimizing (8) but over a complex range of α, either rectangular or circular. However, this complex optimization when applied to the group velocity was found to give very similar results to the real optimization of the group velocity, and so will not be considered further here.

III. Theoretical results

Figure 2 shows the phase error $\varepsilon_p = |\frac{\bar{\alpha}}{\alpha} - 1|$ plotted on a log scale in the complex α plane for stencils created from some of the different optimization methods described above. In order to accentuate the differences, a 15-point ($N = 7$) 4th order ($L = 2$) stencil has been used. All optimizations used for figure 2 involve integration along the real α axis: the classical DRP optimization (3) for figure 2(a); the group velocity optimization (8) for 2(c); and the second derivative optimization (9) for 2(e). Figure 2(a) is exactly the DRP scheme of Tam[10]. By way of comparison, figure 2(b) uses the maximal order (14th order) stencil. The limit of integration η for the optimizations was chosen such that each method gave a comparable error along the real axis in its region of validity, and as can be seen from figure 2 each method achieves an accuracy of 10^{-4} along the real axis. Coefficients for all derivatives given here can be found in appendix A.

The classical DRP scheme in figure 2(a) just gives the best performance for real α, while the second derivative optimization given in figure 2(e) gives the best performance extending off the real axis into the complex α plane; the group velocity optimization of figure 2(c) gives an intermediate result. Figures 2(d,f) compare which derivative is the most accurate (red is maximal order, blue is classical DRP, green is new DRP). As predicted, the classical DRP extends its accuracy the furthest for constant amplitude oscillations (real α), while the group velocity based optimizations are accurate for a wider range of non-constant amplitude oscillations (complex α). Note that, for the parameters of Ref. 14 given by the dashed lines, the maximal order stencil is still the most accurate.

Figure 3 plots the comparable errors for maximizing η subject to a maximum acceptable error in either the group velocity $|\mathrm{d}\bar{\alpha}/\mathrm{d}\alpha - 1| < \varepsilon$, or its derivative $|\mathrm{d}^2\bar{\alpha}/\mathrm{d}\alpha^2| < \varepsilon$, for real $\alpha\Delta x < \eta$. The values of ε were chosen to give comparable phase error along the real α axis, and the results are almost indistinguishable from those from minimizing the errors given η. Again, for the parameters of Ref. 14 given by the dashed lines, the maximal order stencil is still the most accurate.

Finally, figure 4 plots the phase errors resulting from optimizing over ranges of complex α, as shown in figure 1(a): figure 4(a,b) use the rectangular region (4) with $a = 0.5$; while figure 4(c,d) uses the circular sector region (5) with $\beta = \pi/6$, corresponding to growth or decay per wavelength by a factor of $\exp\{2\pi \tan\beta\} \approx 38$. Both schemes perform well for both real and complex α, and both schemes perform better than the maximal order scheme for the parameters of Ref. 14 for between 4 and 6 points per wavelength. The circular sector scheme is perhaps the better of the two, and also has the physical interpretation of its optimization parameter β in terms of growth or decay rate per wavelength.

In conclusion, if simulations are desired with few points per wavelength and a derivative of relative accuracy 10^{-4} is sufficient, the 15-point circular sector derivative used here performs well at five points per wavelength for growth or decay per wavelength up to a factor of 23. While 15 point 4th order stencils have been considered here to exaggerate the differences between the optimization methods, similar results are expected for smaller width stencils. Results for the more common 7 point 4th order stencils are given in appendix A.1.

IV. Practical example

In this section, the 1D wave propagation and damping test case from Ref. 13 is solved using the various derivative schemes given in the previous section. This example problem is intended to test simultaneously both wave propagation with significant damping per wavelength and undamped wave propagation over many wavelengths, with the coefficients inspired by realistic parameters from aeroacoustics[14]. The governing equations

$$\frac{\partial p}{\partial t} + \frac{\partial v}{\partial x} = -k_p(x)p, \tag{10a}$$

$$\frac{\partial v}{\partial t} + \frac{\partial p}{\partial x} = -k_v(x)v, \tag{10b}$$

are solved on a periodic domain $x \in [0, 24)$, depicted in figure 5. Initial conditions consist of a wave packet with wavelength 1 occupying $x \in [2, 18]$, and a region of damping of strength $k_p = k_q = 3$ occupying $x \in [21, 23]$. This gives a complex wavenumber $\alpha = 2\pi - 3\mathrm{i}$ in the damped region and $\alpha = 2\pi$ elsewhere. At time $t = 24$, the initial wave should have propagated exactly once around the periodic x-domain, and by

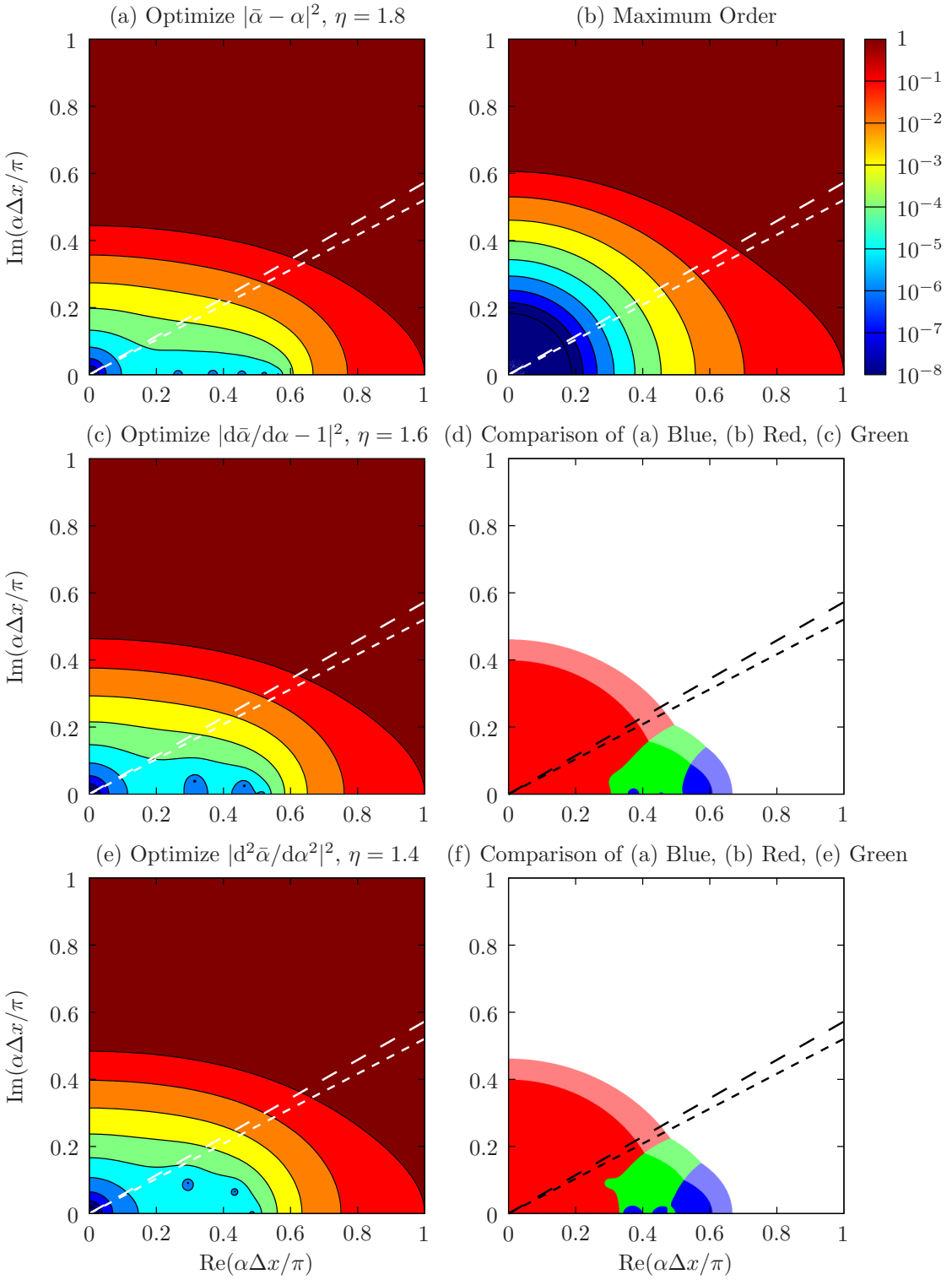

Figure 2: Plots in the complex α plane of phase error $|\bar{\alpha}/\alpha - 1|$ on a log scale, for 15-point ($N = 7$) schemes of 4th order accuracy. (a) is the scheme of Tam[10] using the real-α DRP optimization (3). (c) optimizes group velocity using (8). (e) optimizes using (9). (d) and (f) compare which scheme is most accurate; white means no scheme is 1% accuracy, light colours mean no scheme is 0.1% accurate. The diagonal lines correspond to the axial wavenumbers investigated by Tam, Ju & Chien[14].

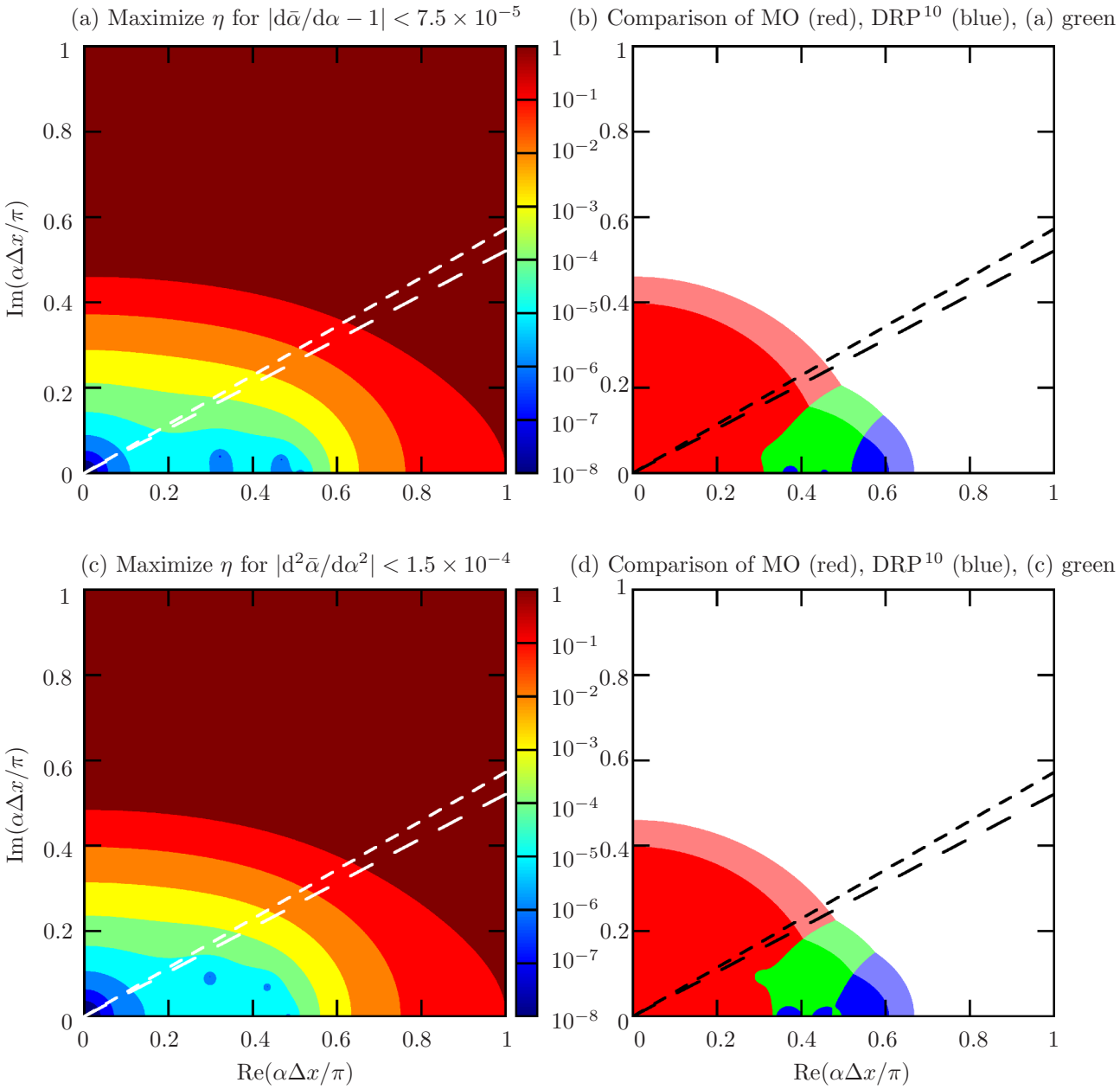

Figure 3: As for figure 2, but for maximizing η subject to the given maximum error constraints. (b) and (d) compare figures 2(a) and 2(b) with (a) and (b) here.

comparing with the analytic solution [13] we define the error in the solution as

$$E = \sup_{x\in[0,24)} \left\{ \left|p(x,0) - \mathrm{e}^6 p(x,24)\right|, \left|v(x,0) - \mathrm{e}^6 v(x,24)\right| \right\}. \tag{11}$$

We investigate the resolution required to achieve $E = 0.01$.

A. Results for 7-point stencils

We first consider for 7-point ($N = 3$) 4th order ($L = 2$) derivatives. Since these derivatives have only one degree of freedom, they may be classified by a single parameter. In this case, they are parameterized by ε, the maximum deviation of their numerical group velocity, such that $|\mathrm{d}\bar{\alpha}/\mathrm{d}\alpha - 1| < \varepsilon$ for $|\alpha\Delta x| < \eta$ for

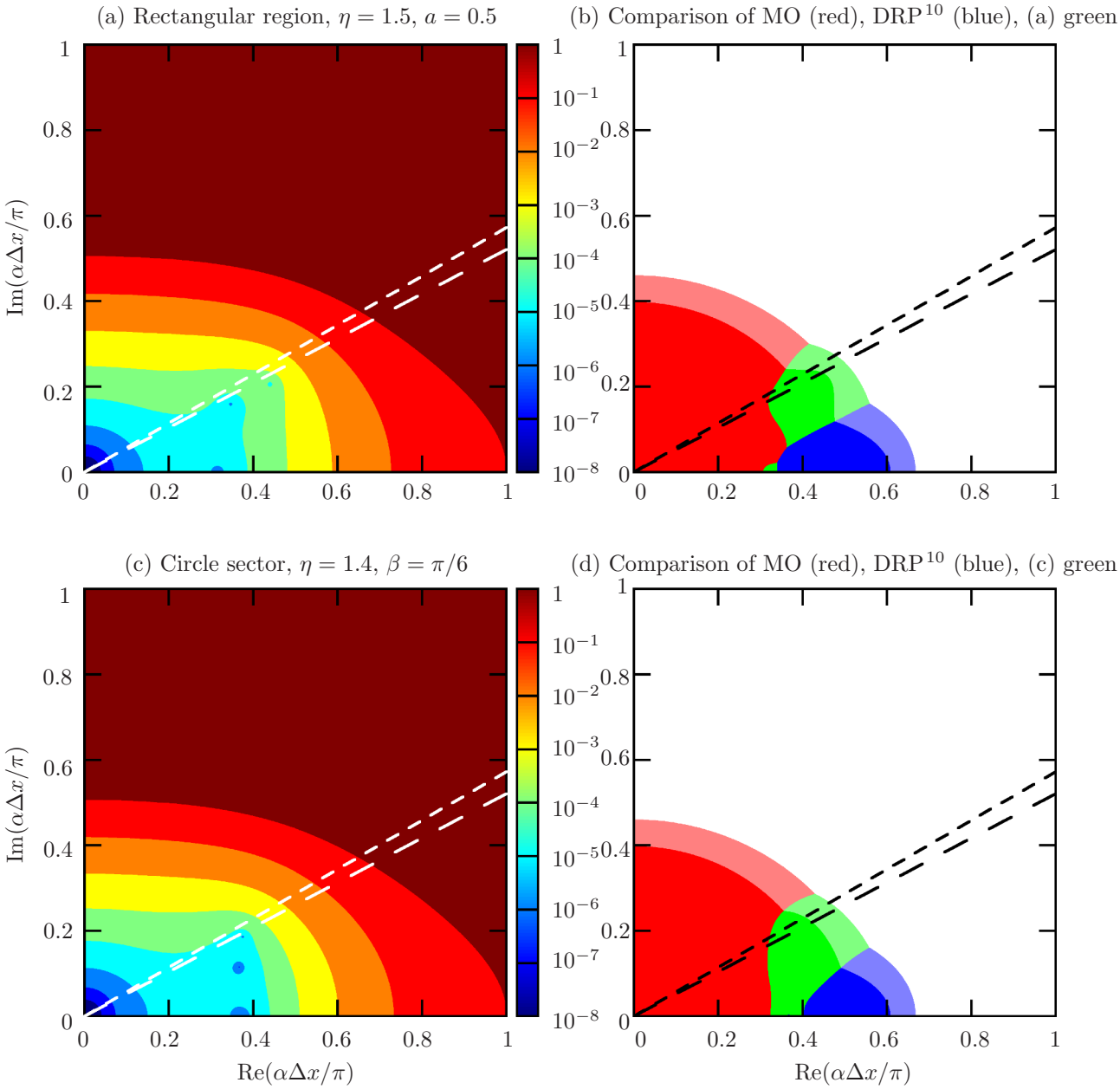

Figure 4: As for figure 2, but for optimizing $|\bar{\alpha} - \alpha|^2$ over a rectangular region (4) or sector of a circle (5). (b) and (d) compare figures 2(a) and 2(b) with (a) and (b) here.

maximal η. The formula for these derivatives is given in appendix A.1. The DRP derivative of Tam & Webb[5] corresponds to $\varepsilon = 2.24 \times 10^{-2}$, while the DRP derivative of Tam & Shen[6] corresponds to $\varepsilon = 2.76 \times 10^{-3}$. The maximal (6th) order derivative is recovered in the limit $\varepsilon \to 0$.

Figure 6 plots the error against points per wavelength (PPW) for a range of such derivatives. In order that the error is dominated by the spatial derivative, a "perfect" adaptive timestep RK45 time integration is used, and similarly a "perfect" spatial filtering using a 19-point 16th order filter is used. The Maximal Order derivative is found to need 14 PPW to achieve $E = 0.01$ accuracy. By comparison, the Tam & Shen[6] derivative needs 20.5 PPW and the Tam & Webb[5] derivative needs 26 PPW, showing that they are clearly over-ambitiously optimized for this test case. The $\varepsilon = 10^{-4}$ derivative performs best for $E = 0.01$, needing 11.5 PPW. If further accuracy were needed, for $E = 10^{-3}$ the best performing derivative is the $\varepsilon = 10^{-5}$ derivative, needing 17 PPW, with the maximal order derivative needing 21 PPW and the previously optimum

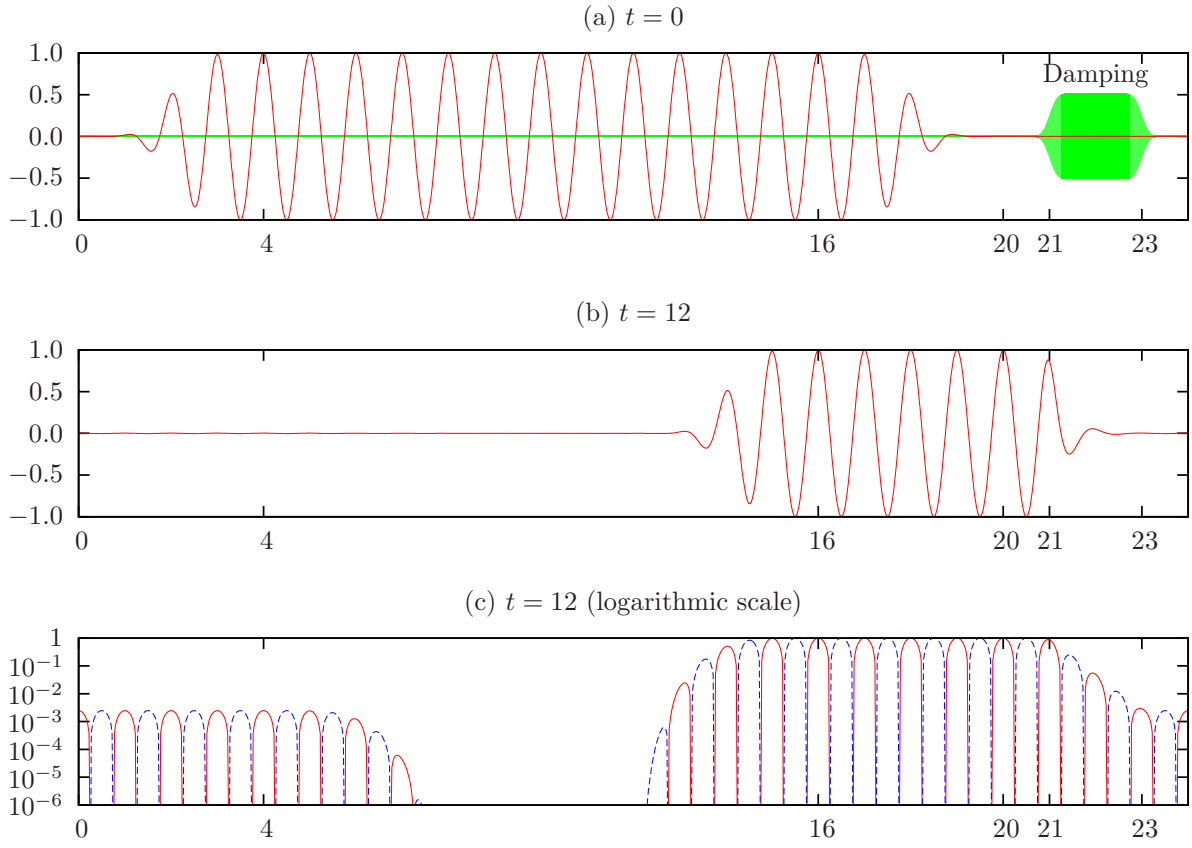

Figure 5: Diagram of the wave problem considered, taken from Fig. 8 of Ref. 13. The domain is periodic in the x-direction. The initial wave in (a) has amplitude 1 for $x \in [4, 16]$ and smoothly decays to zero amplitude for $x \in (0, 4)$ and $x \in (16, 20)$. The damping (rescaled by 1/6) in (a) has equivalent length 2, with full amplitude for $x \in \left[21\frac{1}{2}, 22\frac{1}{2}\right]$ and a smooth decay to zero amplitude for $x \in \left(20\frac{1}{2}, 21\frac{1}{2}\right)$ and $x \in \left(22\frac{1}{2}, 23\frac{1}{2}\right)$. (b) and (c) show the wave at time $t = 12$ on a linear (b) or logarithmic (c) scale. In (c), dashed lines denote negative values and solid lines denote positive values.

$\varepsilon = 10^{-4}$ derivative needing 26 PPW. A general rule of thumb appears to be to use the $\varepsilon = E/100$ derivative if an accuracy of E is required, although this is presumed to be specific to this test case.

If instead of the "perfect" time integration and filtering a more standard LDDRK56[16] time integration and a 7-point 6th order filter are used, the results obtained are as shown in figure 7. In this case, for $E = 0.01$ accuracy the best derivative is again the $\varepsilon = 10^{-4}$ derivative, although this now requires 13 PPW. By comparison, the Maximal Order derivative requires 14.5 PPW, while the existing DRP schemes[5,6] still need 20.5 and 26 PPW. If further accuracy were needed, for $E = 10^{-3}$ the best performing derivative is again the $\varepsilon = 10^{-5}$ derivative, needing 19.5 PPW, with the maximal order derivative needing 22 PPW and the previously optimum $\varepsilon = 10^{-4}$ derivative needing 26 PPW.

These results show that it is possible to use optimized derivatives to achieve a given accuracy with few points per wavelength for this test case, but that existing DRP schemes[5,6] are over-ambitiously optimized and fail to beat the classical maximum order scheme for this test case. Since 7-point 4th order stencils have only one degree of freedom, optimization with different target metrics will still yield a similar result. To compare the different optimization metrics described in section II above, it is therefore necessary to consider wider derivatives with more degrees of freedom.

B. Results for 15-point stencils

Figure 8 plots the error E against the number of points per wavelength for 15-point ($N = 7$) 4th order ($L = 2$) derivatives, again using a "perfect" adaptive time-step RK45 time integrator and a "perfect" 19-

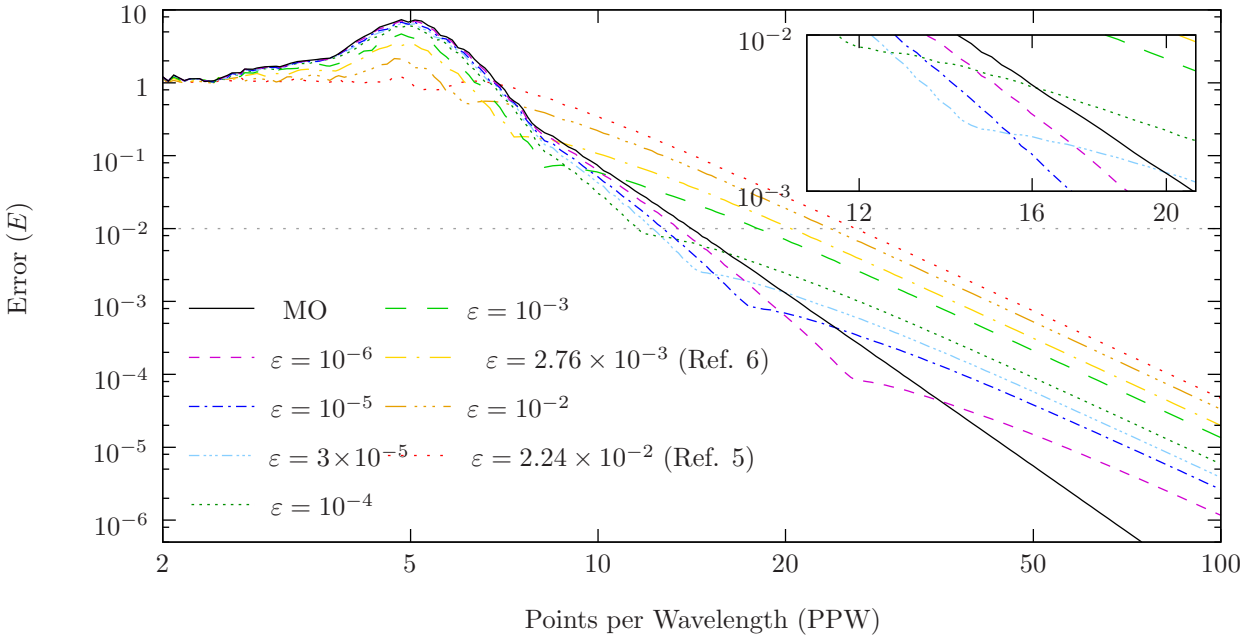

Figure 6: Plot of the error E from (11) against points per wavelength (PPW), for 7-point derivatives given by (14). A "perfect" 19-point 16th order spatial filter and a "perfect" adaptive step RK45 time integration are used.

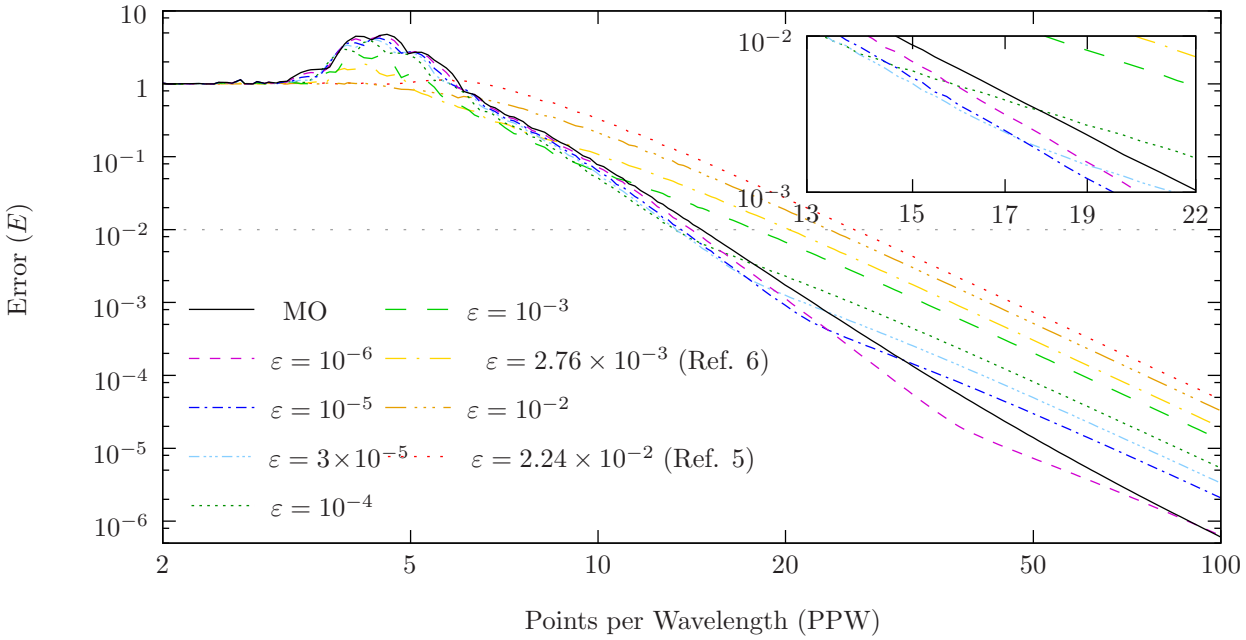

Figure 7: Plot of the error E from (11) against points per wavelength (PPW), as per figure 6, but using the LDDRK56[16] time integration with a CFL number of 0.8, and a standard 7-point 6th order filter.

point 16th order spatial filter so that the error is dominated by the spatial derivatives. The 7-point maximal order and 7-point DRP[6] schemes are also plotted for comparison. Up to 6 PPW, all 15-point schemes are equally accurate; which is to say, poorly accurate. The best schemes achieve $E = 0.01$ with 6.5 PPW, while the 15-point maximal order schemes needs 6.75 PPW and the classical DRP[10] needs 7.2 PPW. However, the accuracy of the optimized schemes then drops off significantly, with $E = 10^{-3}$ achieved by the 15-point MO scheme in 8.2 PPW, while the others need over 15 PPW; the 7-point MO scheme even beats the 17-point DRP[10] scheme, with the former needing 21 PPW and the latter 23.5 PPW to achieve $E = 10^{-3}$.

From this, it would appear that there is little to no advantage, and significant disadvantages, to using a

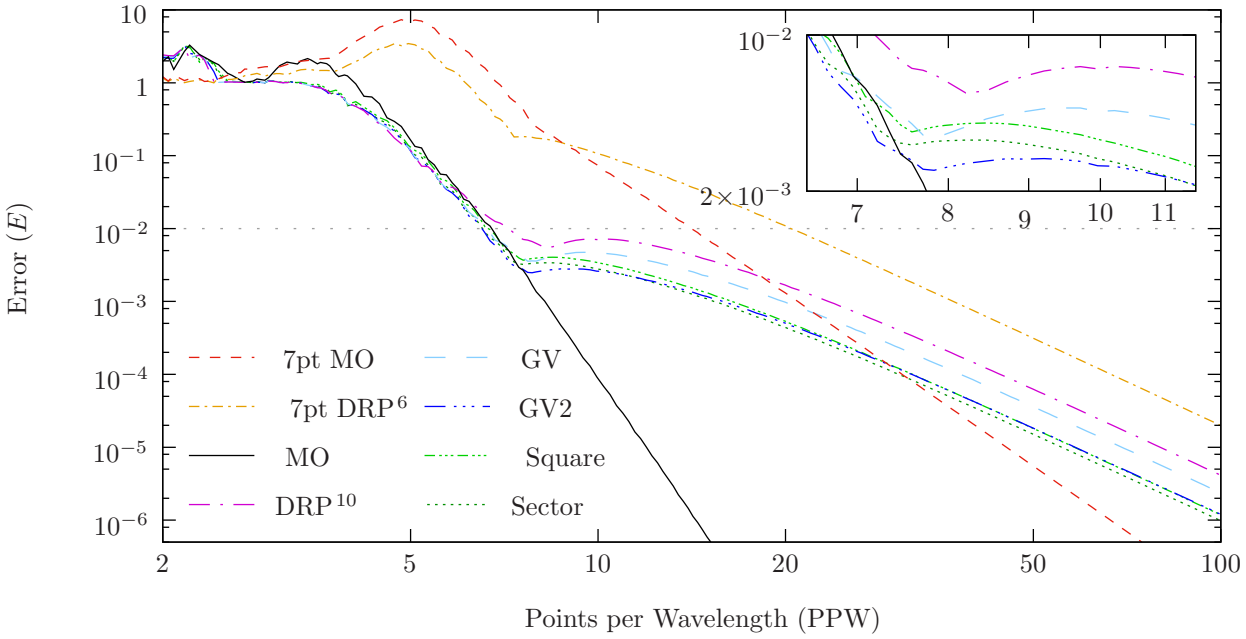

Figure 8: Plot of the error E from (11) against points per wavelength (PPW). All stencils are 15-points wide unless specified. MO = Maximum Order. DRP = Phase-optimized using (3). GV = Group velocity optimized using (8). GV2 = Derivative of group velocity optimized using (9). Square = Phase-optimized using (4). Sector = Phase-optimized using (5). A "perfect" 19-point 16th order spatial filter and a "perfect" adaptive step RK45 time integration are used.

15-point optimized scheme over a 15-point maximal order scheme for this test case. Of the optimized schemes, the GV2 and the Sector schemes perform the best, with the GV2 performing best to around $E = 2.5 \times 10^{-3}$ accuracy (11 PPW), after which the Sector scheme becomes more accurate. The 15-point maximal order scheme has a clear advantage for 7 or more PPW over any of the optimized schemes.

Figure 9 shows a comparable plot to figure 8 of error against points per wavelength, but in this case for the LDDRK56[16] time integration with a fixed CFL number of 0.8. An error of $E = 0.02$ is reached by all 15-point schemes by 8–8.5 PPW. Interestingly, and in contrast to figure 8, beyond this the sector (5), square (4), and derivative of group velocity (9) optimized stencils each perform better than the maximal order stencil, despite figure 8 showing that with "perfect" time integration the maximal order stencil performs better. Of these three, the sector optimized shows the best results, with $E = 2.5 \times 10^{-4}$ being obtain with 16 PPW for the sector stencil, 18 PPW for the group velocity derivative stencil, 19 PPW fro the square stencil, and 21 PPW for the maximal order stencil, with the classical DRP[10] stencil needing 33 PPW for the same accuracy. This indicates a synergy between the spatial derivative and the temporal integration that is not investigated further here. Figure 10 shows that this synergy disappears when the LDDRK56 time integration uses a lower CFL number of 0.2, and the theoretical results of figure 8 are recovered.

V. Conclusion

Explicit symmetric finite difference schemes optimized for non-constant amplitude waves have been considered. Both theoretical and practical comparisons have been made with existing optimized and maximal order schemes. The practical comparisons use the test case of Ref. 13, which solves a wave equation combining propagation over many wavelengths and rapid decay over a few wavelengths, with parameters inspired by aeroacoustics simulations[14]. In general, relatively few optimized schemes outperform the classical maximal order schemes, and even then the out-performance is slight; as predicted previously[13], no existing DRP scheme outperforms their equivalent maximal order scheme.

A number of different ways to optimize finite difference schemes for use with non-constant amplitude waves have been considered here. In addition to the classical DRP optimization of (3), which aims to minimize phase velocity errors for real α (constant amplitude waves), rectangular (4) and circular sector (5)

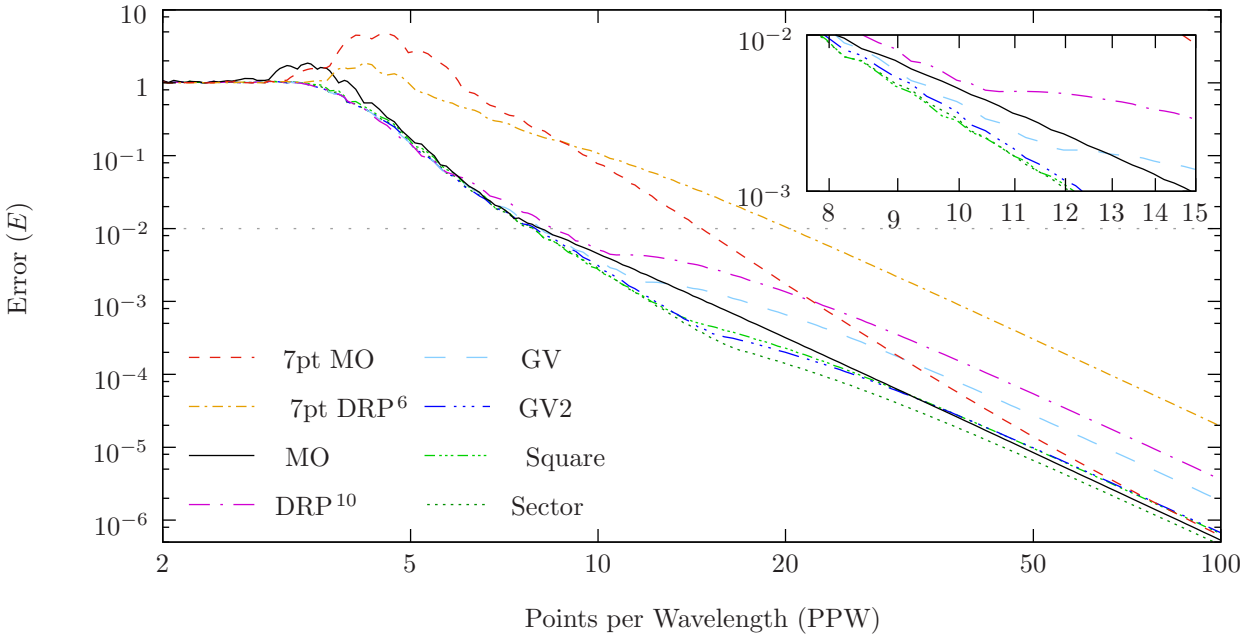

Figure 9: Plot of the error E from (11) against points per wavelength (PPW), as per figure 8, but using the LDDRK56[16] time integration with a CFL number of 0.8. The 7-point stencils also use a standard 7-point 6th order filter.

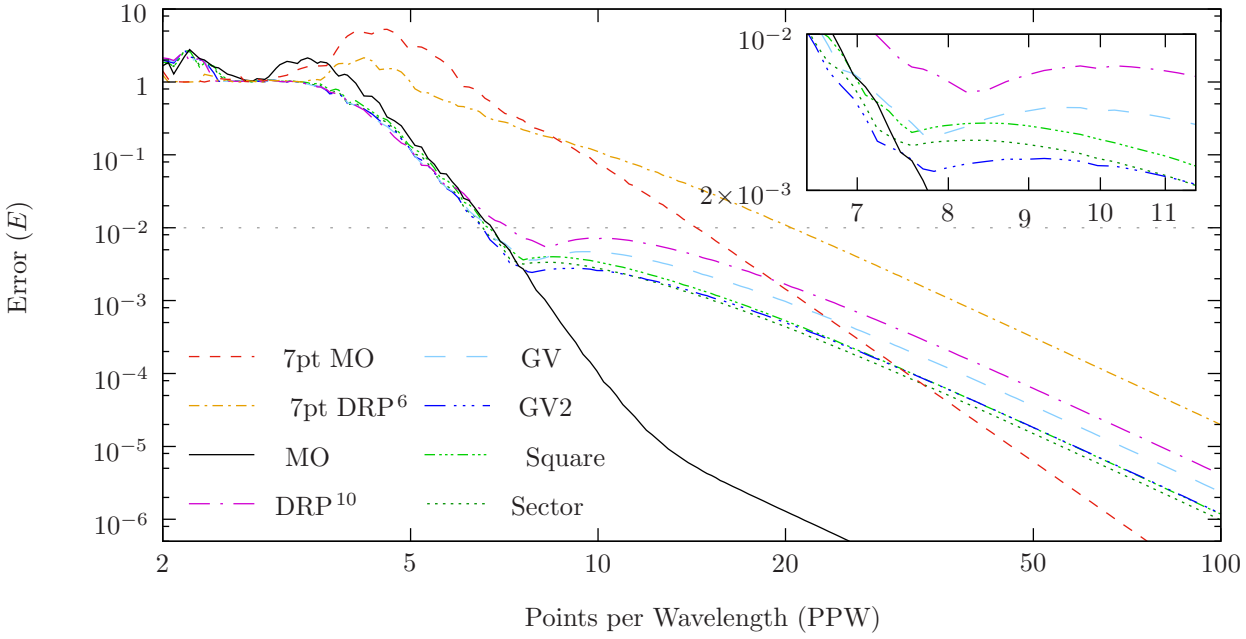

Figure 10: Plot of the error E from (11) against points per wavelength (PPW), as per figure 9, but using the LDDRK56[16] time integration with a CFL number of 0.2.

regions of the complex α plane were also considered (as shown in figure 1(a)), with the circular sector showing the most promise (figures 8 and 9). The circular sector optimization also has the advantage of an interpretation of optimizing over a range of growth- or decay-rates per wavelength, with the $\beta = \pi/6$ angle used here corresponding to a maximum factor of 37 per wavelength. Minimizing group velocity (8) or the derivative of group velocity (9) for real α was also considered, since $\bar{\alpha}(\alpha)$ being a complex differentiable function implies that accurate behaviour of derivatives of $\bar{\alpha}$ along the real α axis lead to accurate behaviour of $\bar{\alpha}$ for complex α in a neighbourhood of the real α axis; this was borne out in practice (figure 2). While

these optimizations were investigated primarily using rather wide 15-point 4th order stencils to exaggerate the effect of the optimization by allowing a large number of degrees of freedom to optimize over, similar results are expected for narrower stencils.

Also considered was minimizing the number of points per wavelength for which the accuracy of the group velocity could be kept within given bounds ($|\mathrm{d}\bar{\alpha}/\mathrm{d}\alpha - 1| < \varepsilon$). For the 15-point stencils this produced nearly identical results to optimizing the group velocity along the real axis. However, for the one-parameter family of 7-point 4th order stencils, the accuracy ε provided a useful parameterization. Using the formula in (14) to calculate such derivatives given ε, a range of derivatives were compared, including the pre-existing DRP schemes of Tam & Webb[5] ($\varepsilon = 2.24 \times 10^{-2}$) and Tam & Shen[6] ($\varepsilon = 2.76 \times 10^{-3}$). In general, as ε is reduced the schemes become less accurate at few points per wavelength for constant-amplitude waves, and more accurate for non-constant-amplitude waves (figure 12); in the limit $\varepsilon \to 0$ the 6th order 7-point derivative is recovered. For the test case of section IV, the pre-existing DRP schemes were found to be over-optimized with too ambitiously large values of ε (figures 6 and 7). Instead, for the test case considered here, for a target error of E an optimized derivative with $\varepsilon = E/100$ appeared to perform best. As one example, to obtain 1% accuracy ($E = 10^{-2}$) in the test case at a CFL number of 0.8, the $\varepsilon = 10^{-4}$ derivative required 13 points per wavelength (PPW), the classical maximal order derivative required 14.5 PPW, while the DRP scheme of Tam & Shen[6] required 20.5 PPW, and that of Tam & Webb[5] required 26 PPW.

Since the optimizations here prioritize particular combinations of growthrate and points per wavelength, it is important to know what wavelengths and growthrates are experienced in actual simulations; for example, the choice of the parameters a and β in (4) and (5) depend on the types of waves likely to be present in simulations. It is also often impractical or undesirable to use differently optimized derivative schemes in different directions (such as axially, radially, and azimuthally in cylindrical geometry), and schemes need to be optimized to perform well in all directions. This complication may well mean that no scheme may be appropriately optimized for all directions, and in such cases the maximal order schemes are likely to behave best, since their performance is independent of $\arg\alpha$ provided there is sufficient resolution such that $|\alpha|$ is sufficiently small.

The results for realistic simulations using the LDDRK56[16] time integration at a CFL number of 0.8 suggest a synergy between the spatial derivatives and temporal integration used (figures 7 and 9), which disappears when the time integration is better resolved (figures 6, 8 and 10). This synergy was also noted in section 3.4 of Ref. 13, and it seems likely that jointly optimizing both the time integration and the spatial derivative together will yield better results than optimizing either of them independently; this was not investigated further here.

Other avenues of future research include extending the results presented here to implicit (i.e. compact) schemes, for which the theory presented here remains valid, or to non-symmetric schemes for use at domain boundaries, a preliminary study of which is given in Ref. 11.

Acknowledgements

E.J. Brambley is grateful for the support of a Royal Society University Research Fellowship.
V.K. Markevičiūtė is grateful for support from the Bridgwater Summer Undergraduate Research scheme.

A. Optimized finite difference coefficients

The coefficients for the 15 point derivative stencils used throughout the paper are given in table 1.

1. A closed form expressions for 7-point stencils with optimized group velocity

For a 7-point 4th order derivative, minimizing the number of points per wavelength subject to a given group velocity accuracy ($\varepsilon_g < \varepsilon$ for $0 \le \alpha \le \eta$) is possible in closed form. We require to solve the simultaneous

Equ.	η	params	d_1	d_2	d_3	d_4
				d_5	d_6	d_7
MO			7/8	-7/24	7/72	-7/264
				7/1320	-7/10296	1/24024
(3)	1.8		9.194250111059936e-1	-3.558295992723656e-1	1.525150160880663e-1	-5.946304083268051e-2
				1.901075271112043e-2	-4.380864930307980e-3	5.389612187866318e-4
(8)	1.6		9.132014790935754e-1	-3.462502387268886e-1	1.433784213097144e-1	-5.323572671744543e-2
				1.596870412088003e-2	-3.406264564626082e-3	3.858154405995108e-4
(9)	1.4		9.070251943909290e-1	-3.369308893850419e-1	1.347767643211234e-1	-4.764054186334629e-2
				1.339660259959042e-2	-2.636946033787389e-3	2.724460105631516e-4
(4)	1.5	$a = 0.5$	8.908414996751749e-1	-3.140867522643636e-1	1.158405871391361e-1	-3.697085728287112e-2
				9.292153980932711e-3	-1.645641713917770e-3	1.581075637816619e-4
(5)	1.4	$\beta = \pi/6$	8.950285192059415e-1	-3.196348336621835e-1	1.199636676314197e-1	-3.894948703892998e-2
				9.901292408553496e-3	-1.752523178812276e-3	1.652529157131945e-4
$\max_{\alpha\in[0,\eta]}\left\{\left\lvert\frac{\mathrm{d}\bar{\alpha}}{\mathrm{d}\alpha}-1\right\rvert<\varepsilon\right\}$			9.136906686290520e-1	-3.470104298158679e-1	1.441213985719431e-1	-5.376082967728889e-2
				1.623902809383762e-2	-3.500449913735769e-3	4.024104298537003e-4
$\max_{\alpha\in[0,\eta]}\left\{\left\lvert\frac{\mathrm{d}^2\bar{\alpha}}{\mathrm{d}\alpha^2}\right\rvert<\varepsilon\right\}$			9.067438894182988e-1	-3.365200922451326e-1	1.344199788770892e-1	-4.742919373407507e-2
				1.331217476313679e-2	-2.616708383926525e-3	2.703585521248940e-4

Table 1: Coefficients of 15-point 4th-order derivative stencils used in this paper. The second row give the derivative of Tam[10]. For row 7, $\varepsilon = 7.5 \times 10^{-5}$. For row 8, $\varepsilon = 1.5 \times 10^{-4}$

equations

$$d_1 + 2d_2 + 3d_3 = \tfrac{1}{2}, \tag{12a}$$

$$d_1 + 8d_2 + 27d_3 = 0, \tag{12b}$$

$$d_1 \sin\alpha_0 + 4d_2 \sin(2\alpha_0) + 9d_3 \sin(3\alpha_0) = 0, \tag{12c}$$

$$d_1 \cos\alpha_0 + 2d_2 \cos(2\alpha_0) + 3d_3 \cos(3\alpha_0) = \frac{1+\varepsilon}{2}, \tag{12d}$$

$$d_1 \cos\eta + 2d_2 \cos(2\eta) + 3d_3 \cos(3\eta) = \frac{1-\varepsilon}{2}. \tag{12e}$$

The first two equations specify 4th order accuracy. The third equation specifies that α_0 is a local maximum of $\mathrm{d}\bar{\alpha}/\mathrm{d}\alpha$, and the fourth specifies that the value taken at that maximum is $1+\varepsilon$. The fifth then gives the value of η, where the minimum number of points per wavelength is given by $\mathrm{PPW} = 2\pi/\eta$, although this is not required to ascertain the stencil coefficients d_1, d_2 and d_3.

Rearranging (12) leads to

$$d_1 = \tfrac{2}{3} + 5d_3, \qquad d_2 = -\tfrac{1}{12} - 4d_3, \qquad \cos\alpha_0 = \frac{1-6d_3}{54d_3}, \tag{13a}$$

$$216000d_3^3 - (10800 + 13122\varepsilon)d_3^2 + 180d_3 - 1 = 0, \qquad \text{or equivalently} \qquad (60d_3-1)^3 = \frac{3^6}{200}\varepsilon(60d_3)^2, \tag{13b}$$

$$72d_3\cos^3\eta - (2+96d_3)\cos^2\eta + (4-24d_3)\cos\eta + 48d_3 - 2 + 3\varepsilon = 0. \tag{13c}$$

Equation (13b) shows that the maximal order scheme is obtained in the limit $\varepsilon \to 0$, with the corresponding coefficient value $d_3 = \frac{1}{60}$. Equation (13b) has solution

$$60d_3 = (1+2\hat{\varepsilon}) + C + 4\hat{\varepsilon}(1+\hat{\varepsilon})/C \quad \text{where} \quad \hat{\varepsilon} = 243\varepsilon/400 \quad \text{and} \quad C = \left(8\hat{\varepsilon}^3 + 12\hat{\varepsilon}^2 + 3\hat{\varepsilon} + \hat{\varepsilon}\sqrt{8\hat{\varepsilon}+9}\right)^{1/3} \tag{14}$$

Figure 11 plots some examples of these optimized schemes for varying values of ε.

Figure 12 compares the 7-point maximal (6th) order derivative to various 7-point 4th order derivatives for non-constant amplitude waves. As ε is reduced, the region of better accuracy of the optimized derivatives increases into the complex α plane, at the expense of its extent along the real α axis. The $\varepsilon = 10^{-4}$ and $\varepsilon = 10^{-5}$ derivatives are found to give particularly good results for the test case in section IV.

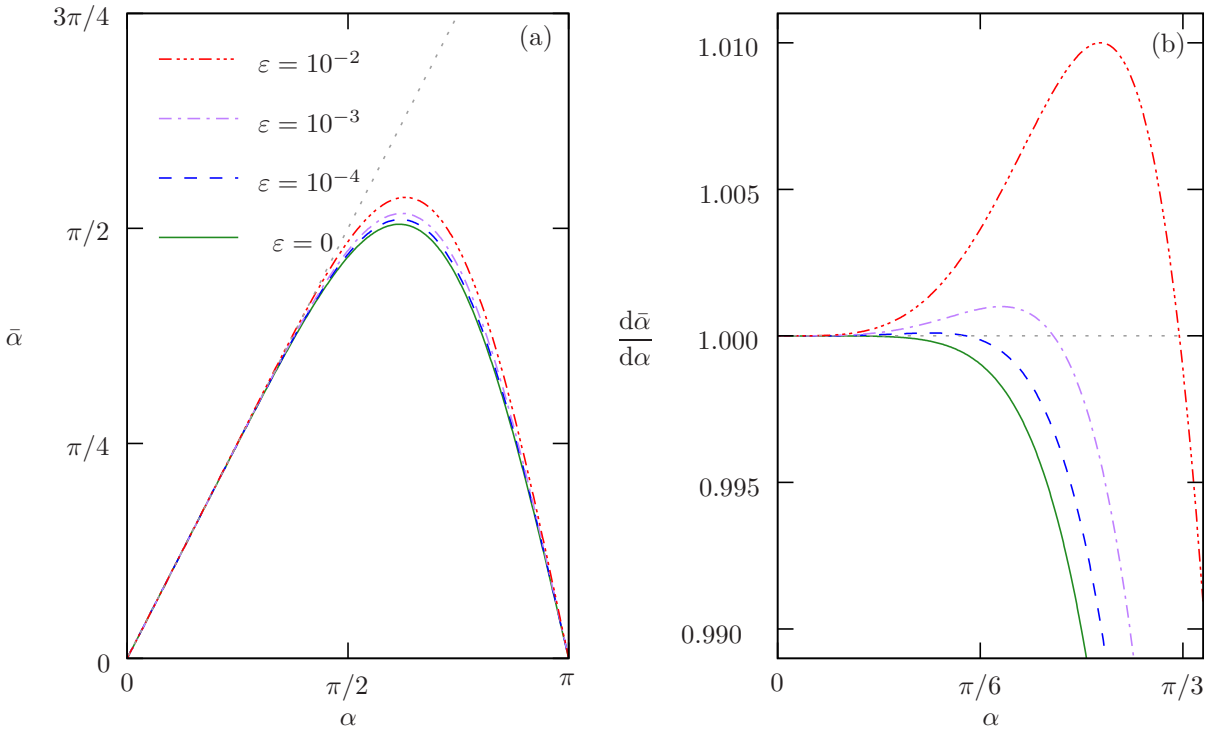

Figure 11: Plots of $\bar{\alpha}(\alpha)$ (a) and $\mathrm{d}\bar{\alpha}/\mathrm{d}\alpha$ (b) for a 7-point 4th order ($N = 3$, $L = 2$) stencil optimized so that $\varepsilon_g < \varepsilon$ for $0 \le \varepsilon \le \eta$ for maximal η. The $\varepsilon = 0$ optimization results in the maximal (6th) order 7-point stencil.

References

[1] Vichnevetsky, R. and De Schutter, F., "A Frequency Analysis of Finite Element Methods for Initial Value Problems," *Advances in Computer Methods for Partial Differential Equations*, edited by R. Vichnevetsky, AICA, Rutgers Univ., New Brunswick, NJ, 1975.

[2] Vichnevetsky, R. and Bowles, J. B., *Fourier Analysis of Numerical Approximations of Hyperbolic Equations*, SIAM, Philadelphia, 1982.

[3] Holberg, O., "Computational Aspects of the Choice of Operator and Sampling Interval for Numerical Differentiation in Large-Scale Simulation of Wave Phenomena," *Geophysical Prospecting*, Vol. 35, 1987, pp. 629–655.

[4] Lele, S. K., "Compact Finite Difference Schemes with Spectral-like Resolution," *J. Comput. Phys.*, Vol. 103, 1992, pp. 16–42.

[5] Tam, C. K. W. and Webb, J. C., "Dispersion-Relation-Preserving Finite Difference Schemes for Computational Acoustics," *J. Comput. Phys.*, Vol. 107, 1993, pp. 262–281.

[6] Tam, C. K. W. and Shen, H., "Direct Computation of Nonlinear Acoustic Pulses using High-Order Finite Difference Schemes," AIAA paper 93-4325, 1993.

[7] Kim, J. W. and Lee, D. J., "Optimized Compact Finite Difference Schemes with Maximum Resolution," *AIAA J.*, Vol. 34, No. 5, 1996, pp. 887–893.

[8] Bogey, C. and Bailly, C., "A Family of Low Dispersive and Low Dissipative Explicit Schemes for Flow and Noise Computations," *J. Comput. Phys.*, Vol. 194, 2004, pp. 194–214.

[9] Kim, J. W., "Optimised Boundary Compact Finite Difference Schemes for Computational Aeroacoustics," *J. Comput. Phys.*, Vol. 225, 2007, pp. 995–1019.

[10] Tam, C. K. W., *Computational Aeroacoustics*, chap. 2, Cambridge, 2012.

[11] Brambley, E. J., "Asymmetric Finite Differences for Non-Constant-Amplitude Waves," *Proc. International Congress on Sound and Vibration, London, 23–27 July*, 2017.

[12] Brambley, E. J., "DRP schemes perform poorly for decaying or growing oscillations," AIAA paper 2015-2540, 2015.

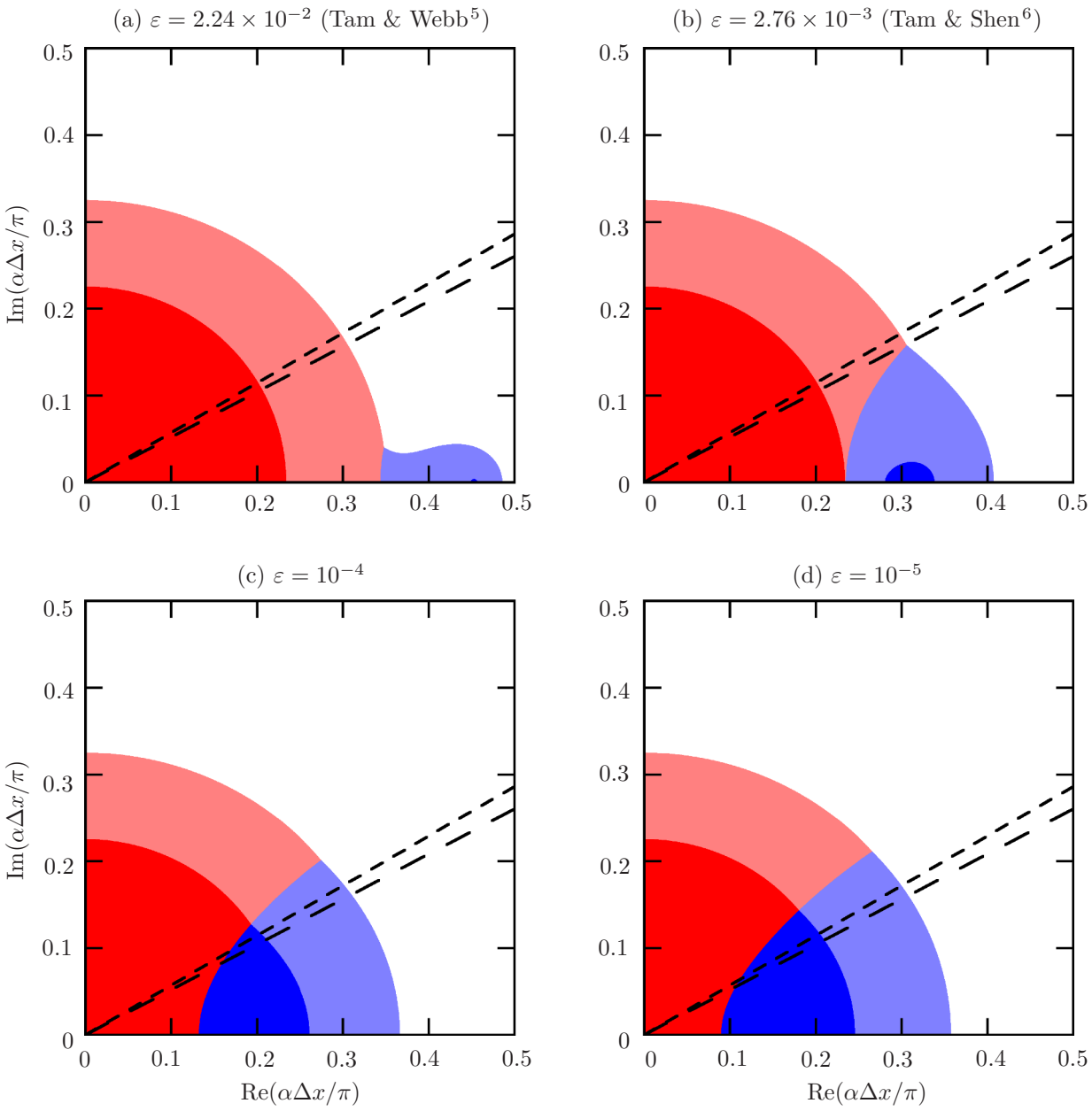

Figure 12: Comparison in the complex α plane of which of the 7-point Maximal Order (red) or the given 7-point 4th order derivative (blue) is the most accurate. White means no scheme is 1% accuracy, light colours mean no scheme is 0.1% accurate. The diagonal lines correspond to the axial wavenumbers investigated by Tam, Ju & Chien[14].

[13] Brambley, E. J., "Optimized finite-difference (DRP) schemes perform poorly for decaying or growing oscillations," *J. Comput. Phys.*, Vol. 324, 2016, pp. 258–274.

[14] Tam, C. K. W., Ju, H., and Chien, E. W., "Scattering of Acoustic Duct Modes by Axial Liner Splices," *J. Sound Vib.*, Vol. 310, 2008, pp. 1014–1035.

[15] Trefethen, L. N., "Group Velocity in Finite Difference Schemes," *SIAM Review*, Vol. 24, No. 2, 1982, pp. 113–136.

[16] Hu, F. Q., Hussaini, M. Y., and Manthey, J. L., "Low-Dissipation and Low-Dispersion Runge–Kutta Schemes for Computational Acoustics," *J. Comput. Phys.*, Vol. 124, 1996, pp. 177–191.